

Onset of Nuclear Matter Expansion in Au+Au Collisions

P. Crochet^{1*}, F. Rami¹, A. Gobbi², R. Donà^{1,3}, J.P. Coffin¹, P. Fintz¹, G. Guillaume¹,
F. Jundt¹, C. Kuhn¹, C. Roy¹, B. de Schauenburg¹, L. Tizniti¹, P. Wagner¹, J.P. Alard⁴,
V. Amouroux⁴, A. Andronic⁵, Z. Basrak⁶, N. Bastid⁴, I. Belyaev⁷, D. Best², J. Biegansky⁸,
A. Buta⁵, R. Čaplar⁶, N. Cindro⁶, P. Dupieux⁴, M. Dželalija⁶, Z.G. Fan⁴, Z. Fodor⁹,
L. Fraysse⁴, R.P. Freifelder², N. Herrmann², K.D. Hildenbrand², B. Hong², S.C. Jeong²,
J. Kecskemeti⁹, M. Kirejczyk¹⁰, P. Koncz⁹, M. Korolija⁶, R. Kotte⁸, A. Lebedev^{7,11},
Y. Leifels², V. Manko¹¹, D. Moisa⁵, J. Mösner⁸, W. Neubert⁸, D. Pelte¹², M. Petrovici⁵,
C. Pinkenburg², P. Pras⁴, V. Ramillien⁴, W. Reisdorf², J.L. Ritman², A.G. Sadchikov¹¹,
D. Schüll², Z. Seres⁹, B. Sikora¹⁰, V. Simion⁵, K. Siwek-Wilczyńska¹⁰, U. Sodan²,
K.M. Teh², M. Trzaska¹², M. Vasiliev¹¹, G.S. Wang², J.P. Wessels², T. Wienold²,
K. Wisniewski², D. Wohlfarth⁸, A. Zhilin⁷

(FOPI Collaboration)

¹*Centre de Recherches Nucléaires, IN2P3-CNRS, Université Louis Pasteur, Strasbourg, France*

²*Gesellschaft für Schwerionenforschung, Darmstadt, Germany*

³*Istituto Nazionale di Fisica Nucleare, Legnaro, Italy*

⁴*Laboratoire de Physique Corpusculaire, IN2P3-CNRS, Université Blaise Pascal,
Clermont-Ferrand, France*

⁵*Institute for Physics and Nuclear Engineering, Bucharest, Romania*

⁶*Ruđer Bošković Institute, Zagreb, Croatia*

⁷*Institute for Theoretical and Experimental Physics, Moscow, Russia*

⁸*Forschungszentrum Rossendorf, Dresden, Germany*

⁹*Research Institute for Particles and Nuclear Physics, Budapest, Hungary*

¹⁰*Institute of Experimental Physics, Warsaw University, Warsaw, Poland*

¹¹*Russian Research Institute “Kurchatov”, Moscow, Russia*

*Present address : GSI, Darmstadt, Germany

Abstract

Using the FOPI detector at GSI Darmstadt, excitation functions of collective flow components were measured for the Au+Au system, in the reaction plane and out of this plane, at seven incident energies ranging from $100A$ MeV to $800A$ MeV. The threshold energies, corresponding to the onset of sideward-flow (balance energy) and squeeze-out effect (transition energy), are extracted from extrapolations of these excitation functions toward lower beam energies for charged products with $Z \geq 2$. The transition energy is found to be larger than the balance energy. The impact parameter dependence of both balance and transition energies, when extrapolated to central collisions, suggests comparable although slightly higher values than the threshold energy for the radial flow. The relevant parameter seems to be the energy deposited into the system in order to overcome the attractive nuclear forces.

Keywords : Heavy ion collisions, nuclear matter expansion, sideward-flow, squeeze-out, radial flow, balance energy, transition energy.

PACS numbers : 25.70.-z, 25.75.Ld

I. INTRODUCTION

Collective motions of nuclear matter occurring in heavy ion collisions are of great interest since they are expected to provide information about the properties of hot and dense nuclear matter and the underlying equation of state (EoS) [1]. Flow effects were predicted by hydrodynamical calculations [1,2] and experimentally evidenced at LBL-BEVALAC [3]. At beam energies $E_{\text{lab}} \geq 200A$ MeV, the interaction between nuclei is dominated by individual nucleon-nucleon scattering and the repulsive component of the mean field. This leads to a collective deflection of matter to positive angles in the reaction plane *i.e.* in the direction of the projectile remnants (sideward-flow). Conversely, at few tens of A MeV, the interaction is dominated by the attractive mean field, so that nucleons emitted in the reaction plane are deflected to negative angles [4]. At a certain intermediate incident energy, named the balance energy E_{BAL} , the attractive component and the repulsive component of the interactions balance each other and consequently the flow crosses zero, changing from a negative sign at low energies to a positive sign at high energies. The balance effect was extensively investigated at GANIL [5–7] and MSU [8–11] by measuring different colliding systems. It was also studied in the framework of theoretical models [12–24]. For semi-central collisions, the balance energy was found to be sensitive to the stiffness of the nuclear EoS and to the in-medium reduction of the nucleon-nucleon cross section [13]. At lower impact parameters the balance energy is expected to be only sensitive to the in-medium nucleon-nucleon cross section [13,20]. Recent experimental results [25–28] revealed also, in the same beam energy range, signatures of a change in the azimuthal emission pattern of mid-rapidity particles, from an in-plane enhancement at low incident energies to the well known out-of-plane preferential emission, the so-called squeeze-out [29,30], at higher energies. The incident energy where this transition takes place (termed E_{TRA}) is also found to be sensitive to the in-medium nucleon-nucleon cross section [28].

The excitation functions of both sideward-flow and squeeze-out effects were measured with the FOPI detector [31] for the Au+Au system at seven incident energies between $E_{\text{lab}} =$

100A MeV and $E_{\text{lab}} = 800A$ MeV. The ability of the FOPI device to detect intermediate mass fragments ($Z \geq 3$) allows a cleaner identification of the collective flow signal and a better extrapolation of the measured excitation functions of the in-plane and of the out-of-plane flows toward their thresholds at low incident energies. We found however that the threshold energies are rather insensitive to the charge of the considered particles ($Z > 1$). We found also that the transition point seems to be located at higher beam energies than the balance point. On the other hand, the FOPI detector ensures a wide range of impact parameter collisions to be explored. This offers the possibility to investigate the centrality dependence of E_{BAL} and E_{TRA} , an aspect which was recognized to be crucial in this kind of study [11,13,23]. This allows us to discuss for the first time this centrality dependence in conjunction with the threshold energy (E_{RAD}) for the radial flow in highly central collisions. It shows that the three threshold energies (E_{BAL} , E_{TRA} , and E_{RAD}) might be attributed to a common phenomenon, the relevant parameter being the energy deposited into the nuclear system.

II. EXPERIMENTAL SETUP

The data presented in this paper concern the Au+Au system at seven incident energies $E_{\text{lab}} = 100, 120, 150, 250, 400, 600$ and $800A$ MeV. They have been collected with the Phase I of the FOPI detector [31] at the SIS/ESR accelerator facility, GSI Darmstadt. In its Phase I configuration, the FOPI detector covers in full azimuth the laboratory polar angles (Θ_{lab}) from 1.2° to 30° . It consists mainly of a highly segmented Forward Wall of plastic scintillators divided into two parts : the Inner Wall made of 252 trapezoidal scintillators which covers the Θ_{lab} range between 1.2° and 7.5° , and the Outer Wall made of 512 scintillator strips which covers the Θ_{lab} domain from 7° to 30° . The Forward Wall provides an element identification and the velocity of the reaction products through energy loss and time-of-flight measurements. Its segment structure allows to determine the velocity vector components. A complementary shell of 188 thin energy loss detectors is mounted

in front of the Forward Wall in order to achieve lower detection thresholds. This cluster detector is made of an ensemble of gas-filled ionisation chambers (Parabola) mounted in front of the Outer Wall, and thin plastic scintillator paddles (Rosace) combined with the Inner Wall. In order to reduce the background scattering in the air gas, a helium bag is placed between the target and the detectors. This setup measures simultaneously most of the light charged particles and intermediate mass fragments (up to $Z = 15$) emitted in the forward center-of-mass (c.m.) hemisphere. Its high granularity allows high multiplicity events to be measured with a negligible multi-hit rate. The apparatus ensures a very good azimuthal symmetry which is an important feature for the study of the flow phenomena.

III. EVENT CHARACTERISATION

A. Impact parameter determination

The measured events were sorted according to their degree of centrality using the standard method based on the correlation between the multiplicity of emitted particles and the impact parameter. The multiplicity distribution of the charged particles detected in the Outer Wall exhibits the typical plateau for intermediate values, followed by a steep decrease at the highest multiplicities [32]. The highest multiplicity bin (named PM5) has been defined by cutting at half of the plateau value (the corresponding lower limits of the PM5 multiplicity bin are given in Tab.I). The remaining part of the multiplicity distribution has been subdivided into four equally spaced bins (named PM1 to PM4) according to the procedure used by the Plastic Ball Collaboration [33]. The results presented in what follows include only events belonging to the PM3-PM5 multiplicity classes where background contamination, estimated from measurements without target, is negligible. The mean impact parameter associated to each PM event class has been determined in the framework of the IQMD (Isospin Quantum Molecular Dynamics) model [16,34] by filtering the theoretical calculations with the realistic simulator of the FOPI detector. The resulting $\langle b \rangle$ values

and their r.m.s deviations are presented in Tab. II for the beam energies $E_{\text{lab}} = 150$ and $400A$ MeV. Note that $\langle b \rangle$ values are the same within the r.m.s deviations at the other beam energies. It can be seen from Tab. II that the multiplicity criterium offers a large coverage of the impact parameter range. On the other hand, model studies [35], using the so-called quality factor introduced by Cugnon and L'Hôte [36], allowed us to show that with the FOPI/Phase-I setup, the multiplicity criterium, as compared to other criteria, appears as the most appropriate one for exploring flow observables over a large impact parameter domain.

B. Reaction plane reconstruction

The reaction plane was reconstructed with the transverse momentum analysis devised by Danielewicz and Odyniec [37]. In order to remove autocorrelation effects, the azimuth of the reaction plane was estimated for each particle i in a given event as the plane containing the vector \vec{Q}_i and the beam axis, where \vec{Q}_i is calculated from the transverse momenta \vec{p}_t^j of all detected particles except the particle i :

$$\vec{Q}_i = \sum_{\substack{j=1 \\ j \neq i}}^M \omega^j (\vec{p}_t^j + m^j \vec{v}_b^i).$$

M is the multiplicity of the event and $\omega^j = 1$ if $y_j^{(0)} > \delta$, -1 if $y_j^{(0)} < -\delta$ and 0 otherwise. $y_j^{(0)}$ is the j^{th} particle rapidity divided by the projectile rapidity in the c.m. system. The parameter δ , chosen equal to 0.5 , was introduced in order to remove mid-rapidity particles which have a negligible correlation with the reaction plane. According to [38], a boost velocity $\vec{v}_b^i = \vec{p}_t^i / (m^{\text{sys}} - m^i)$ (m^i is the mass of the particle i and m^{sys} is the sum of the projectile and target masses) was applied to each particle j in order to take into account the effects of momentum conservation due to the exclusion of the particle i . The influence of these effects on the observables considered in the present work was found to be of a few percent at the lowest beam energies ($E_{\text{lab}} = 100$ and $120A$ MeV) and negligible at higher incident energies.

The accuracy of the reaction plane reconstruction (*i.e.* the azimuthal deviation $\Delta\Phi_R$ of the reconstructed reaction plane with respect to the true one) was estimated for each event class by randomly dividing each event into two equal parts and by taking the one half of the angle between the \vec{Q} vectors of the two subevents [37]. The azimuthal dispersion $\sigma(\Delta\Phi_R)$ was found to vary typically from $\sim 20^\circ$ to $\sim 40^\circ$ for the PM event classes under consideration. It is worth noting that the use of a heavy system such as Au+Au offers, in the beam energy range considered here, a good event characterisation both in centrality and reaction plane reconstruction as compared to lighter systems whose measured ejectile multiplicities are lower.

IV. RESULTS AND DISCUSSION

A. Sideward-flow

The in-plane flow component (sideward-flow) is examined in terms of the normalized in-plane transverse momentum $p_x^{(0)}$ ($p_x^{(0)} = (p_x/A)/p_{c.m.}^p$, where p_x/A is the in-plane transverse momentum per nucleon and $p_{c.m.}^p$ is the projectile momentum per nucleon in the c.m. system) as a function of the normalized c.m. rapidity $y^{(0)}$ ($y^{(0)}$ is defined above). This normalisation, suggested in earlier works [39,40], is motivated by the fact that one obtains a scale invariant representation of the data in a fluid dynamical description of the collision. Figure 1 shows a typical example of $p_x^{(0)}$ (Fig. 1.a) and $\langle p_x^{(0)} \rangle$ (Fig. 1.b) *versus* $y^{(0)}$ plots for $Z = 4$ particles detected in semi-central (PM4) reactions at $E_{lab} = 250A$ MeV. Since the experimental apparatus covers only the forward c.m. hemisphere, the plot has been measured for positive $y^{(0)}$ rapidities and reflected for negative ones. As shown by Fig. 1.b, the dependence of $\langle p_x^{(0)} \rangle$ on $y^{(0)}$ exhibits the well known S-shape behavior [37] demonstrating the collective transfer of momentum between the backward and the forward hemispheres. The linear part of the curve in the participant region (*i.e.*, at mid-rapidity) reflects the so-called side-splash effect while the fall-off starting just below the projectile rapidity ($y^{(0)} = 1$)

is caused by the bounce-off effect [41]. A quantitative measure of the amount of flow in the participant region of the collision is given by the so-called normalized flow parameter $F_S^{(0)}$ which is commonly defined as the slope of the $\langle p_x^{(0)} \rangle$ versus $y^{(0)}$ curve at mid-rapidity [42] : $F_S^{(0)} = d \langle p_x^{(0)} \rangle / dy^{(0)} \Big|_{y^{(0)} \simeq 0}$. Technically the $F_S^{(0)}$ parameter is obtained by fitting a polynomial function of the form : $a + F_S^{(0)} \times y^{(0)} + c \times (y^{(0)})^3$ to the data (Fig. 1.b). The fit was restricted to the linear branch of the S-shape curve. As shown in reference [37], because the particle momenta are not projected onto the true reaction plane, their projections are on average biased downward by a factor $1 / \langle \cos(\Delta\Phi_R) \rangle$ where $\Delta\Phi_R$, as mentioned before, is the estimate of the azimuthal deviation of the reconstructed reaction plane with respect to the true one. The data shown in Fig. 1.b and all the $F_S^{(0)}$ values presented in what follows are corrected for this effect. The correction factors ($1 / \langle \cos(\Delta\Phi_R) \rangle$) were typically ranging from 1.10 to 1.45 depending on the beam energy and the multiplicity bin.

The precise evaluation of the acceptance effects on the in-plane flow is rather difficult due to the complexity of the different experimental constraints. This can only be investigated in the framework of realistic simulations where theoretical calculations are passed through the detector filter. In this context, we have used the IQMD model [16,34] which is known to reproduce quite well experimental flow data [43–48]. A few thousand of IQMD events were generated over a large range of impact parameters with the HM choice (Hard EoS plus a momentum dependent potential) of the nuclear interaction. This force is recognized as providing the best description of the observed trends in the in-plane flow data [44–47]. For the present study, theoretical events were filtered applying geometrical cuts and energy thresholds of the FOPI detector. They were presorted in accordance with the above mentioned procedure used for the data (see before). The in-plane flow was extracted with respect to the true reaction plane which is known in the model. Because of the limited statistics, apparatus effects could only be evaluated for light particles. We found that the experimental cuts only slightly affect $\langle p_x^{(0)} \rangle$ values in the forward c.m. hemisphere. The observed deviations are mainly caused by the geometrical limit of detection at $\Theta_{\text{lab}} = 30^\circ$. This cut biases down the $F_S^{(0)}$ parameter by about 20% for $Z = 1$ and by less than 10% for

heavier particles in the PM5 event class at $E_{\text{lab}} = 250A$ MeV. Note that these effects decrease with increasing fragment size [49] because heavy particles, due to their low sensitivity to thermal fluctuations, occupy a smaller phase space. Therefore, in order to avoid misleading interpretations of the data, the $F_S^{(0)}$ flow parameters presented in what follows include only the measurements of particles whose charge is ≥ 2 . On the other hand, it is worth noting that the effects of the $\Theta_{\text{lab}} = 30^\circ$ cut decreases with increasing impact parameters since peripheral and semi-central event topologies are less accentuated in the transverse direction as compared to central events.

B. Squeeze-out

The out-of-plane flow component was investigated from the azimuthal distributions $dN/d\Phi$ (Φ is the azimuthal angle of the detected particle relative to the azimuth of the reaction plane) around the beam axis of mid-rapidity particles, selected by imposing a rapidity cutoff $-0.1 < y^{(0)} < 0.1$. It is now an established fact that the out-of-plane anisotropy increases strongly with the transverse momentum of charged particles [50–52]. Therefore, in order to extract relevant information from the data, we determined the squeeze-out signal by choosing a p_t cut which, within the acceptance, gives access to the largest momenta and sufficiently wide for statistics considerations. This p_t window is $0.4 < p_t^{(0)} < 0.55$, $p_t^{(0)}$ being the particle transverse momentum per nucleon divided by the projectile momentum per nucleon in the c.m. system. These rapidity and transverse momentum cuts used to extract the signal, define a portion of the phase space which is covered by the FOPI detector acceptance [51]. Figure 2 shows a typical $dN/d\Phi$ distribution for $Z = 3$ particles in the PM4 event class at an incident energy of $E_{\text{lab}} = 250A$ MeV. A clear preferential emission is observed in the direction perpendicular to the reaction plane ($\Phi = 90^\circ$ and $\Phi = 270^\circ$). This enhanced emission reflects the squeeze-out effect. The magnitude of the latter is commonly defined as the ratio R_N of the number of particles emitted perpendicular to the reaction plane to the number of particles emitted in the reaction plane [30,53] :

$R_N = (N(90^\circ) + N(270^\circ)) / (N(0^\circ) + N(180^\circ))$. The R_N ratio is extracted by fitting a function of the form $N(\Phi) = a_0 + a_1 \times \cos(\Phi) + a_2 \times \cos(2\Phi)$ to the data (curve of Fig. 2). Thus R_N is calculated as $R_N = (a_0 - a_2) / (a_0 + a_2)$. According to this definition, $R_N < 1$ and $R_N > 1$ are related to a preferential emission of matter in the reaction plane and out of this plane, respectively while $R_N = 1$ corresponds to a perfect azimuthally isotropic situation. The anisotropy ratio R_N can be corrected, like the flow parameter $F_S^{(0)}$, for the uncertainties due to fluctuations of the reaction plane [30]. However, we found with the help of simulations that, for the low multiplicity events, the values of $\langle \cos^2(\Delta\Phi_R) \rangle$, which are the quantities involved in these corrections, were not determined with good accuracy. Thus, R_N ratios reported in what follows are not corrected for the effects of reaction plane fluctuations. Nevertheless, the possible influence of these effects on the observed trends will be discussed in the following.

C. Balance energy

Figure 3 shows the excitation functions of the scale invariant flow parameter $F_S^{(0)}$ for different particles ($Z = 2$ to 5). A sudden decrease is observed in the incident energy region $E_{\text{lab}} < 200 \text{ A MeV}$. It is interesting to notice that this sudden change is much more pronounced in the case of the heavier fragments which are more sensitive to the collective motion. An extrapolation with Fermi functions allows us to estimate the balance energy (intersection with the abscissa) for different types of particles. Note that the balance energy values extracted from extrapolations of the data with other functions, such as logarithmic and second order polynomial ones, were found to be the same within error bars [35]. We have also verified that the use of other scaling variables for the in-plane transverse momentum, such as $\langle p_x / p_t \rangle$ (as used in [54]) or $\langle p_x \rangle / \langle p_t \rangle$, leads to very similar results. The extrapolation for $Z = 3$ fragments leads to an intersection energy of $E_{\text{BAL}} = 65 \pm 15 \text{ A MeV}$ for events corresponding to the PM4 bin. The resulting values for the other particles ($Z = 2, 4$ and 5) are the same within uncertainties as the one obtained for $Z = 3$

(see Tab. III). This confirms the observations established by studying lighter systems that the balance energy is independent of the size of the detected particle [9,10]. Our present balance energy point is somewhat larger than the one obtained for the same system from other experiments [54,55]. This is probably due to the fact that our PM4 event class contains less central events than the one used in references [54,55]. Indeed, as it is shown in the following, the balance energy is found to decrease with decreasing impact parameters. With this in mind, the balance energy value extracted here is consistent with the systematics of the balance energy as a function of the mass of the combined projectile-target system obtained from MSU and GANIL results [56]. On the other hand, it is worth noting that for a heavy system like Au+Au, because of the strong Coulomb repulsion, the overall force is always repulsive [23]. Since the balance energy should correspond to the energy at which the attractive and repulsive component of the nuclear interaction balance each other, it must be evaluated without contamination of non nuclear contribution to the flow. For light systems this problem is less severe because of the much weaker Coulomb repulsion. Nevertheless, for heavy systems one may hope to extract the correct value of the balance energy by extrapolating the $F_S^{(0)}$ values from sufficiently high energies where Coulomb contribution is negligible.

D. Transition energy

The dependence of the anisotropy ratio R_N on the collision impact parameter is presented in Fig. 4 at four incident energies going from 100 to 400A MeV. The signal includes here the contributions of all detected particles each weighted by its charge. By doing so we reconstruct a coalescence invariant quantity which makes meaningful the investigation of the anisotropy ratio as a function of the impact parameter and the beam energy. The geometrical impact parameter b_g was obtained from the measured multiplicity distributions by assuming a sharp-cut-off approximation. This allows us to perform direct comparisons of data measured at different bombarding energies. As can be seen in Fig. 4, the correlation

between the R_N ratio and the impact parameter exhibits a very different trend as the incident energy decreases. At the highest bombarding energy ($400A$ MeV) one can observe a bell-shaped distribution whose maximum is located at intermediate impact parameters (close to $6fm$). It is worth noting that the results obtained at higher energies are quite similar to those observed at $E_{lab} = 400A$ MeV [57]. With decreasing beam energies, the shape of the correlation evolves gradually toward a different trend which is an evidence for a clear change in the emission pattern. Thus at $E_{lab} = 100A$ MeV, with decreasing impact parameter, one observes a transition from a preferential in-plane emission ($R_N < 1$) to the squeeze-out effect characterized by an enhanced out-of-plane emission ($R_N > 1$).

Before going to the interpretations of this behaviour, it must be pointed out that two effects might influence the R_N ratio : i) the dispersion of the reconstructed reaction plane with respect to the true one, which tends to attenuate the magnitude of the signal and ii) the sideward-flow deflection which favors the emission of particles in the reaction plane. In both cases the magnitude of the effect is impact parameter and beam energy dependent. Therefore, in order to eliminate possible ambiguities in the interpretation of the experimental observations in Fig. 4, it was necessary to examine the respective influences of these effects on the correlation between the anisotropy ratio and the impact parameter. A further complete analysis of the data has allowed us to show that the bell-like shape of the distribution observed at high beam energies is preserved after taking into account both mentioned effects [57]. On the other hand, the transition from $R_N > 1$ to $R_N < 1$ at $E_{lab} = 100A$ MeV cannot be caused by one of these two effects. Indeed, fluctuations of the reaction plane tend to attenuate an anisotropy signal regardless of whether the R_N ratio is larger or smaller than 1. Therefore, taking into account the corresponding corrections in Fig. 4, the transition effect would be even more pronounced. On the other hand, an extraction of the R_N quantity around the flow axis would shift up the experimental points but at large b_g 's, where the in-plane enhancement is observed, the flow angle is expected to be fairly low [35] in particular at the lowest beam energy ($E_{lab} = 100A$ MeV) which is close to the balance energy (Fig. 3).

Let us now go back to the interpretations of the experimental observations of Fig. 4.

At high energies, the maximum located near $b_g = 6fm$ is consistent with an expansion-shadowing picture, *i.e.* an expansion of the compressed matter in the central region of the collision which is hindered by the presence of cold spectator remnants. It is worth noting that recent IQMD calculations for neutrons [58] predict a similar bell-shaped correlation with a maximum around $7fm$. At low incident energies ($E_{lab} \leq 150A$ MeV), a clear evidence for a transition from an enhanced in-plane emission pattern to a preferential out-of-plane emission is observed when b_g decreases. The results show that this transition takes place close to $E_{lab} = 100A$ MeV for collisions with impact parameters $b_g \simeq 6fm$. This effect was already observed for a lighter system [25] and very recently for the same system Au+Au [28]. It might be attributed to a change from a collective rotational behaviour governed by the attractive mean field at low energies, to the high energy squeeze-out effect resulting from the repulsive pressure built up during the high density stage of the collision [25,28].

The transition energy E_{TRA} , corresponding to an azimuthally symmetric distribution ($R_N = 1$), can be evaluated from the excitation function of the anisotropy ratio R_N . This has been already investigated in a previous analysis [51] where the experimental E_{TRA} values were compared to the predictions of the IQMD model. The excitation functions of the R_N ratio are presented in Fig. 5 for $Z = 2$ and 3 particles emitted in semi-central (PM4) collisions. Since events were selected here over a large multiplicity bin, the large statistics allowed us to investigate the anisotropy signal in a reduced high p_t window as compared to the previous one. This p_t condition (fixed as $0.5 < p_t^{(0)} < 0.55$) was chosen in order to extract from the data the largest R_N magnitudes within the acceptance of the detector. As one can see from Fig. 5, the R_N ratio tends to saturate above $E_{lab} = 250A$ MeV and seems possibly to decrease at higher energies. On the other hand, the behaviour of the signal at low beam energies exhibits the same sudden change as in the case of the excitation functions of the sideward flow.

In order to extract the transition energy, the data points in the beam energy range 100-400A MeV were fitted with a Fermi function (curves of Fig. 5). The values of E_{TRA} ,

reported in Tab. IV, were determined for $Z = 2$ and 3 particles at the intercept of $R_N = 1$ with the curves. Note that the intersection energies were found to be quite insensitive to the form of the fitting function. They seem to be, as observed in the case of the balance energy, independent of the type of the detected particle within the error bars. It can be seen from the results presented in Tab. III and Tab. IV that the transition energy for the PM4 event class ($E_{\text{TRA}} \simeq 100A \text{ MeV}$) is somewhat larger than the corresponding balance energy ($E_{\text{BAL}} \simeq 65A \text{ MeV}$). This finding agrees with recent theoretical calculations for the Ca+Ca system [23]. It could be explained by angular momentum effects or by the fact that at the balance point the compression is not high enough to generate an enhanced out-of-plane emission.

On the other hand, the R_N ratio, which increases with the particle transverse momentum for $E_{\text{lab}} \geq 150A \text{ MeV}$ [50–52], has been extracted over a narrow p_t window ($0.5 < p_t^{(0)} < 0.55$). This could suggest that the extracted transition energy is p_t dependent. Nevertheless, as shown by the insert in Fig. 5, at $E_{\text{lab}} = 100A \text{ MeV}$ where the transition effect takes place, the R_N ratio remains nearly close to 1 in the whole explored $p_t^{(0)}$ domain. Finally, as mentioned before, the R_N ratios are not corrected for fluctuations of the reconstructed reaction plane because the $\langle \cos^2(\Delta\Phi_R) \rangle$ values cannot be accurately determined. Therefore, in order to estimate how the transition energy could be influenced by these fluctuations, we have extracted E_{TRA} from the R_N values obtained by correcting the measured anisotropy ratios using the $\langle \cos^2(\Delta\Phi_R) \rangle$ factors calculated for filtered IQMD theoretical events, where the true reaction plane is known. The resulting transition energy value, for $Z = 3$ particles, was found to be $E_{\text{TRA}} = 111 \pm 10A \text{ MeV}$ in the PM4 event class. This value is very close to the one obtained without correction (Tab. IV).

E. Centrality dependence of threshold energies

The balance and transition energies extracted from extrapolations of the measured $F_S^{(0)}$ and R_N excitation functions in the three different PM multiplicity bins are shown in Fig. 6 as

a function of the collision centrality. E_{BAL} and E_{TRA} are expressed here not in terms of the projectile energy but of the corresponding energy in the c.m. system. They were obtained, due to considerations of detector acceptance effects and statistics, from the measured excitation functions of $Z = 3$ for E_{BAL} and $Z = 2$ for E_{TRA} . As it can be seen, the transition energy is larger than the balance energy over the whole explored impact parameter range. Both threshold energies E_{BAL} and E_{TRA} increase with increasing impact parameters. Such a behaviour has been also very recently observed in the case of the balance energy of the Ar+Sc system [11] and is predicted by the IQMD model for the Ca+Ca system [23]. This increase of E_{BAL} and E_{TRA} with b may indicate that the threshold of flow effects is related to the energy deposited locally into the overlap zone of the collision : if the local temperature is large enough, the generated pressure can overcome the attractive nuclear forces. When going from peripheral to central collisions, the deposited energy becomes larger and the onset of flow is therefore expected to take place at a lower incident energy. At bombarding energies close to the Fermi energy, the participant picture is not well developed like at higher energies and the local temperature depends sensitively on the local heat relaxation-time and on collision time. With this in mind, it is interesting to compare the threshold energies in finite impact parameter collisions with the threshold energy for the radial expansion in central collisions. The latter was determined in reference [59] by extrapolating the excitation function of the mean radial flow velocity, measured in central collisions, toward low incident energies. Its value was found to be about $E_{\text{RAD}} = 35 \pm 10A \text{ MeV}$ [59] which corresponds to a c.m. energy of $8.7 \pm 2.5A \text{ MeV}$. Note that this value is consistent with recent results for the Au+Au reaction obtained at $E_{\text{lab}} = 35A \text{ MeV}$ [60]. Now, considering again Fig. 6, a rough linear extrapolation of our balance and transition energy points toward $\langle b \rangle = 0$ leads to values of $12 \pm 6A \text{ MeV}$ and $16 \pm 5A \text{ MeV}$, respectively. These values are close to each other and consistent with the value of E_{RAD} within the error bars. It is still premature to go to more quantitative interpretations because of the large experimental uncertainties. Nevertheless, it is tempting to speculate on the basis of the observations in Fig. 6 on a common phenomenon at the origin of radial flow, sideward-flow and squeeze-out effects which takes place for the

same deposited energy : when nuclear matter is heated above a certain limit, the attractive nuclear forces are counterbalanced by the thermal pressure and the system starts to expand above this threshold at which the overall force becomes repulsive. This expansion of nuclear matter tends to an azimuthally symmetric pattern (radial flow) in highly central collisions, while in semi-central collisions the expanding matter is pushed to the side (sideward-flow) and the presence of cold spectator remnants hinders participant nucleons to escape in the reaction plane, which gives rise to a preferential out-of-plane emission (squeeze-out). This scenario for the squeeze-out effect is consistent with the observed correlation between the anisotropy ratio and the impact parameter (Fig. 4). Differences on the various threshold energies can be expected on the bases of effects like collision geometry, system size, Coulomb contribution, angular momentum dissipation, non equilibrium dynamics, *etc.* On the other hand, it is worth noting that the c.m. energy of 8.74 MeV where the radial flow sets in, is close to the one of the caloric curve, reported by the ALADIN Collaboration [61,62], where the temperature grows strongly again after the presently debated plateau. As pointed out in ref. [40], this observation suggests that the onset of flow could be interpreted as a possible signature of a liquid-gas phase transition. Indeed, as discussed before, the onset of flow phenomena indicates a change in the reaction scenario from a global repulsive mechanism to a global attractive mechanism when decreasing the incident energy. In a fluid dynamical vision of the collision, it could also be seen as a manifestation of a liquid-gas phase transition since this leads to a sudden decrease of the repulsive pressure and, consequently, of the flow magnitude.

V. CONCLUSION

Collective effects of nuclear matter in Au+Au collisions at incident energies ranging from 100A MeV to 800A MeV were measured for light particles and intermediate mass fragments with the FOPI detector at GSI. The centrality and beam energy dependence of both sideward-flow and squeeze-out effects were investigated. The evolution of the squeeze-out

magnitude R_N with the impact parameter is found to change drastically with the incident energy. At high incident energies the squeeze-out signal exhibits a bell-shape with a maximum located at intermediate impact parameters. This trend is consistent with an expansion-shadowing scenario where the expansion of highly compressed participant nuclear matter is hindered by the presence of cold spectator remnants. At low energies, the data show clearly a transition from an in-plane preferential emission to an out-of-plane enhancement when the centrality increases. This phenomenon might be attributed to a change from a collective rotational motion for large impact parameters to the squeeze-out effect for smaller impact parameters [25,28]. The balance and transition energies, corresponding to the onset of sideward-flow and squeeze-out effects, respectively, have been evaluated from extrapolations toward lower beam energies of the excitation functions of the scale invariant flow parameter $F_S^{(0)}$ and the anisotropy ratio R_N . Both of them are found to be, within errors, independent of the size of the detected particle. The transition energy is larger than the balance energy. The extrapolation of the centrality dependence of both threshold energies toward $b = 0$ leads to a value which is close to the threshold energy for the radial expansion in central collisions. This suggests that the same phenomenon could be at the origin of the three processes. The relevant parameter seems to be the energy deposited into the system in order to counterbalance the attractive nuclear forces although compression effects can also be present. In central collisions the repulsive pressure is expected to be the highest and the participant matter can expand freely in all directions, while for $b \neq 0$, besides complex geometrical and dynamical effects, the presence of the spectator matter causes the appearance of sideward-flow and squeeze-out. Comparisons of the present experimental results with transport model predictions should provide interesting information about the in-medium reduction of the nucleon-nucleon cross section [13,20,28].

ACKNOWLEDGEMENT

This work was supported in part by the French-German agreement between GSI and IN2P3/CEA and by the PROCOPE-Program of the DAAD.

REFERENCES

- [1] H. Stöcker, J.A. Maruhn and W. Greiner, Phys. Rev. Lett. **44** (1980) 725
- [2] W. Scheid, H. Müller and W. Greiner, Phys. Rev. Lett. **32** (1974) 741
- [3] see for example H.H. Gutbrod, A.M. Poskanzer and H.G. Ritter, Rep. Prog. Phys. **52** (1989) 1267 and references therein
- [4] M.B. Tsang *et al.*, Phys. Rev. Lett. **57** (1987) 2720
- [5] J.P. Sullivan *et al.*, Phys. Lett. B **149** (1990) 8
- [6] J. Peter, Nucl. Phys. A **545** (1992) 173c
- [7] W.Q. Shen *et al.*, Nucl. Phys. A **551** (1993) 333
- [8] D. Krofcheck *et al.*, Phys. Rev. Lett. **63** (1989) 2028
- [9] C.A. Ogilvie *et al.*, Phys. Rev. C **42** (1990) R10
- [10] G.D. Westfall *et al.*, Phys. Rev. Lett. **71** (1993) 1986
- [11] R. Pak *et al.*, Phys. Rev. C **54** (1996) 2457
- [12] J.J. Molitoris and H. Stöcker, Phys. Lett. B **162** (1985) 47
- [13] H.M. Xu, Phys. Rev. Lett. **67** (1991) 2769
- [14] H.M. Xu, Phys. Rev. C **46** (1992) R389
- [15] V. de la Mota *et al.*, Phys. Rev. C **46** (1992) 677
- [16] C. Hartnack, Thesis, Frankfurt University, Germany (1992)
- [17] H.M. Xu, Phys. Rev. C **47** (1993) 891
- [18] D. Klakov, G. Welke and W. Bauer, Phys. Rev. C **48** (1993) 1982
- [19] B.A. Li, Phys. Rev. C **48** (1993) 2415

- [20] H. Zhou, H. Li and Y. Zhuo, Phys. Lett. B **318** (1993) 19
- [21] Y. Ma, W. Shen, J. Feng and Y. Ma, Z. Phys. **344** (1993) 469
- [22] H. Zhou, H. Li and Y. Zhuo, Phys. Rev. C **50** (1995) R2664
- [23] S. Soff *et al.*, Phys. Rev. C **51** (1995) 3320
- [24] E. Lehmann *et al.*, Z. Phys. **355** (1996) 55
- [25] R. Popescu *et al.*, Phys. Lett. B **331** (1994) 285
- [26] W.K. Wilson *et al.*, Phys. Rev. C **51** (1995) 3136
- [27] A. Buta, M. Petrovici, L. Legrand, D. Moisa, V. Simion and the FOPI Collaboration, GSI report 95-1 (1995) p. 57
- [28] M.B. Tsang *et al.*, Phys. Rev. C **53** (1996) 1959
- [29] H.H. Gutbrod, K.H. Kampert, B.W. Kolb, A.M. Poskanzer, H.G. Ritter, and H.R. Schmidt, Phys. Lett. B **216** (1989) 267
- [30] M. Demoulin *et al.*, Phys. Lett. B **241** (1990) 476
- [31] A. Gobbi and the FOPI Collaboration, Nucl. Inst. Meth. A **324** (1993) 156
- [32] J.P. Alard and the FOPI Collaboration, Phys. Rev. Lett. **69** (1992) 889
- [33] K.G.R. Doss *et al.*, Phys. Rev. C **32** (1985) 116
- [34] C. Hartnack, J. Aichelin, H. Stöcker and W. Greiner, Phys. Lett. B **336** (1994) 131
- [35] P. Crochet, Thesis, Strasbourg University, France (1996)
- [36] J. Cugnon and D. L'Hôte, Nucl. Phys. A **397** (1983) 519
- [37] P. Danielewicz and G. Odyniec, Phys. Lett. B **157** (1985) 146
- [38] C.A. Ogilvie *et al.*, Phys. Rev. C **40** (1989) 2592

- [39] N. Balázs, B. Schürmann, K. Dietrich and L.P. Csernai, Nucl. Phys. A **424** (1984) 605
- [40] A. Bonasera and L.P. Csernai, Phys. Rev. Lett. **59** (1987) 630
- [41] H.A. Gustafsson *et al.*, Phys. Rev. Lett. **52** (1984) 1590
- [42] K.G.R. Doss *et al.*, Phys. Rev. Lett. **57** (1986) 302
- [43] F. Rami *et al.*, XXXI International Winter Meeting on Nuclear Physics, Bormio (1993)
p. 200
- [44] V. Ramillien and the FOPI Collaboration, Nucl. Phys. A **587** (1995) 802
- [45] T. Wienold, Thesis, Heidelberg University, Germany (1993)
- [46] P. Crochet and the FOPI Collaboration, in preparation
- [47] R. Donà and the FOPI Collaboration, in preparation
- [48] W. Reisdorf and the FOPI Collaboration, Nucl. Phys. A **612** (1997) 493
- [49] P. Crochet and the FOPI Collaboration, GSI report 95-1 (1994) p. 51
- [50] D. Brill *et al.*, Z. Phys. A **355** (1996) 61
- [51] N. Bastid and the FOPI Collaboration, accepted for publication in Nucl. Phys. A
- [52] L. Lambrecht *et al.*, Z. Phys. A **350** (1994) 115
- [53] H.H. Gutbrod, K.H. Kampert, B.W. Kolb, A.M. Poskanzer, H.G. Ritter, R. Schicker
and H.R. Schmidt, Phys. Rev. C **42** (1990) 640
- [54] W.M. Zhang *et al.*, Phys. Rev. C **42** (1990) R491
- [55] M.D. Partlan *et al.*, Phys. Rev. Lett. **75** (1995) 2100
- [56] A. Buta *et al.*, Nucl. Phys. A **584** (1995) 397
- [57] P. Crochet *et al.*, XXXIV International Winter Meeting on Nuclear Physics, Bormio

(1996) p. 421

[58] S.A. Bass, C. Hartnack, H. Stöcker and W. Greiner, preprint, GSI-94-12 (1994)

[59] A. Gobbi, XIV International Joliot-Curie School of Nuclear Physics, Maubuisson, France (1995)

[60] M. D'Agostino *et al.*, Phys. Lett. B **368** (1996) 259

[61] J. Pochodzalla *et al.*, Phys. Rev. Lett. **75** (1995) 1040

[62] G. Papp and W. Nörenberg, AHP Heavy Ion Physics **1** (1995) 241

TABLES

TABLE I. Lower limit $PM5_1$ of the PM5 multiplicity bin at the different beam energies.

E_{lab} (A MeV)	100	120	150	250	400	600	800
PM5 ₁	28	31	36	44	55	62	70

TABLE II. Mean impact parameter $\langle b \rangle$ for each experimental PM multiplicity bin at incident energies of 150 and 400A MeV. $\langle b \rangle$ is determined in the framework of the IQMD model with a hard momentum dependent interaction. Errors represent the r.m.s. deviation of the b distributions.

Multiplicity bin	PM3	PM4	PM5
$E_{\text{lab}}=150A$ MeV	8.8 ± 1.9	5.0 ± 1.9	3.4 ± 1.4
$E_{\text{lab}}=400A$ MeV	7.0 ± 1.1	4.1 ± 1.5	3.2 ± 1.1

TABLE III. Balance energy for $Z = 2$ to 5 particles under the PM4 multiplicity cut (see text). Errors correspond to systematic uncertainties.

Z	2	3	4	5
E_{BAL} (A MeV)	56.0 ± 21.4	65.2 ± 14.9	68.3 ± 11.1	64.5 ± 15.1

TABLE IV. Transition energy for $Z = 2$ and 3 particles under the PM4 multiplicity cut (see text). Errors correspond to statistical uncertainties only.

Z	2	3
$E_{\text{TRA}} (A \text{ MeV})$	98.9 ± 7.6	107.0 ± 6.9

FIGURES

FIG. 1. Upper panel : Normalized in-plane transverse momentum $p_x^{(0)}$ versus the normalized c.m. rapidity $y^{(0)}$ for $Z = 4$ particles detected in semi-central (PM4) Au+Au collisions at $E_{\text{lab}} = 250A$ MeV. The plot is obtained by assuming a forward/backward symmetry. The different grey levels correspond to different linear cuts in multiplicity. The $\Theta_{\text{c.m.}} = 30^\circ$ cut is represented by the solid white curves.

Lower panel : Mean normalized in-plane transverse momentum $\langle p_x^{(0)} \rangle$ as a function of $y^{(0)}$ for $Z = 4$ particles detected in semi-central (PM4) Au(250A MeV)+Au collisions. The data (open stars) are measured only for $y^{(0)} > 0$ and then reflected around the origin (full stars). Data points are larger than the corresponding statistical uncertainties. The solid curve is the result of the fit described in the text.

FIG. 2. Azimuthal distribution of mid-rapidity ($-0.1 < y^{(0)} < 0.1$) $Z = 3$ particles measured in semi-central PM4 collisions at $E_{\text{lab}} = 250A$ MeV. Φ is the particle azimuthal angle around the beam axis, with respect to the reaction plane. The distribution is extracted with the transverse momentum cut $0.4 < p_t^{(0)} < 0.55$. The solid curve is the result of the fit described in the text. Error bars correspond to statistical uncertainties.

FIG. 3. Excitation functions of the normalized flow parameter $F_S^{(0)}$ measured for different particles ($Z = 2$ to 5) in semi-central PM4 collisions. The values are corrected for fluctuations of the estimated reaction plane. The solid lines correspond to the fits to the data points from $E_{\text{lab}} = 100$ to 400A MeV with Fermi functions. Error bars correspond to systematic uncertainties, estimated to 20, 20, and 10% for $E_{\text{lab}} = 100, 120,$ and 150A MeV, respectively and less than 10% for $E_{\text{lab}} \geq 250A$ MeV. These errors are larger than statistical uncertainties.

FIG. 4. Anisotropy ratio R_N as a function of the geometrical impact parameter b_g for Au+Au collisions at $E_{\text{lab}} = 100A$ MeV (crosses), 150A MeV (triangles), 250A MeV (squares) and 400A MeV (circles). R_N includes the contributions of all detected particles with $0.4 < p_t^{(0)} < 0.55$, each being weighted by its charge. Error bars correspond to statistical uncertainties.

FIG. 5. Excitation functions of the R_N ratio for $Z = 2$ (crosses) and $Z = 3$ particles (triangles) detected in semi-central PM4 collisions under the condition $0.5 < p_t^{(0)} < 0.55$. The curves represent the results of a fit with a Fermi function to the data points from $E_{\text{lab}} = 100$ to $400A$ MeV. The insert shows the $p_t^{(0)}$ dependence of the R_N ratio at an incident energy of $100A$ MeV. Error bars correspond to statistical uncertainties.

FIG. 6. Impact parameter dependence of the c.m. threshold energies E_{BAL} (circles) and E_{TRA} (triangles), determined from the measurements of $Z = 3$ and $Z = 2$ particles, respectively. $\langle b \rangle$ has been determined within simulations using the IQMD model at $E_{\text{lab}} = 150A$ MeV (see Tab.2). The dotted lines are linear fits to the data. Horizontal error bars represent the r.m.s. deviation of b distributions. Vertical error bars correspond to systematic and statistical errors for E_{BAL} and E_{TRA} , respectively.

Figure 1

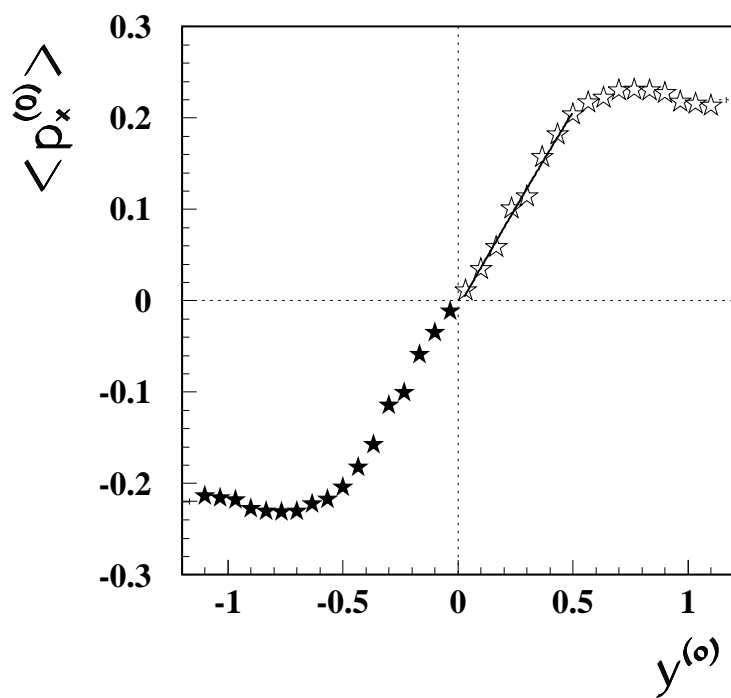
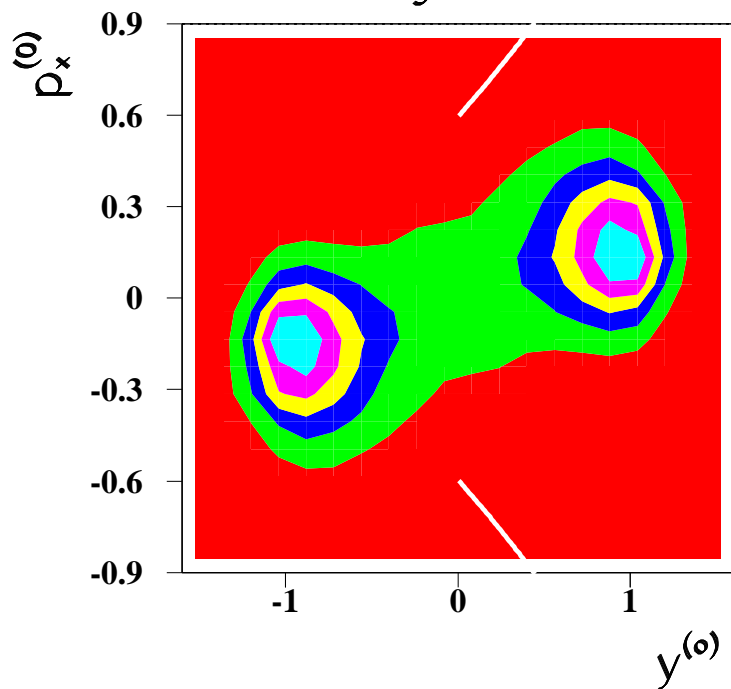


Figure 2

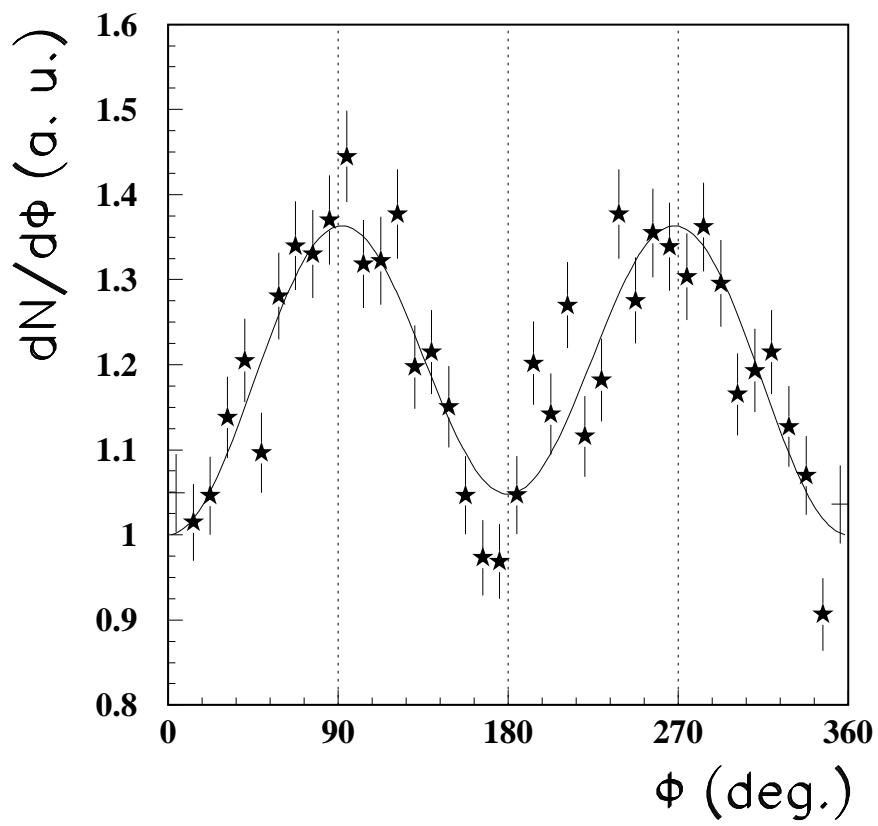


Figure 3

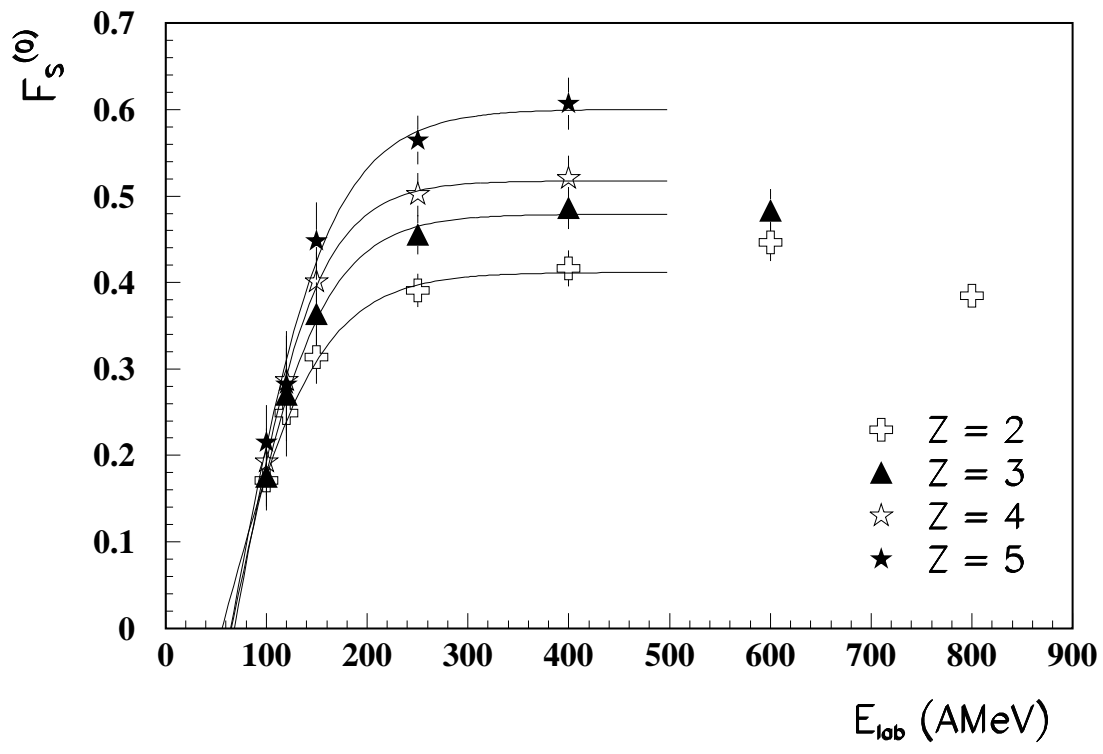


Figure 4

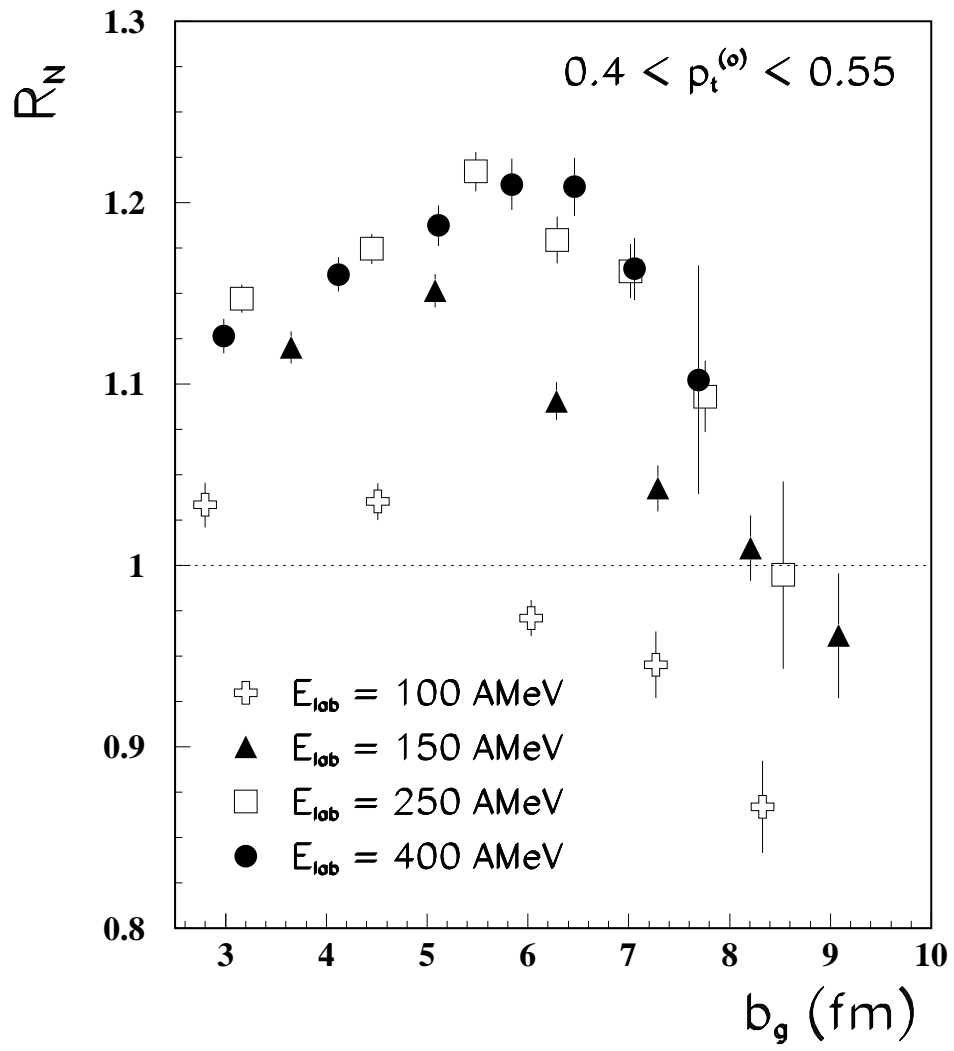


Figure 5

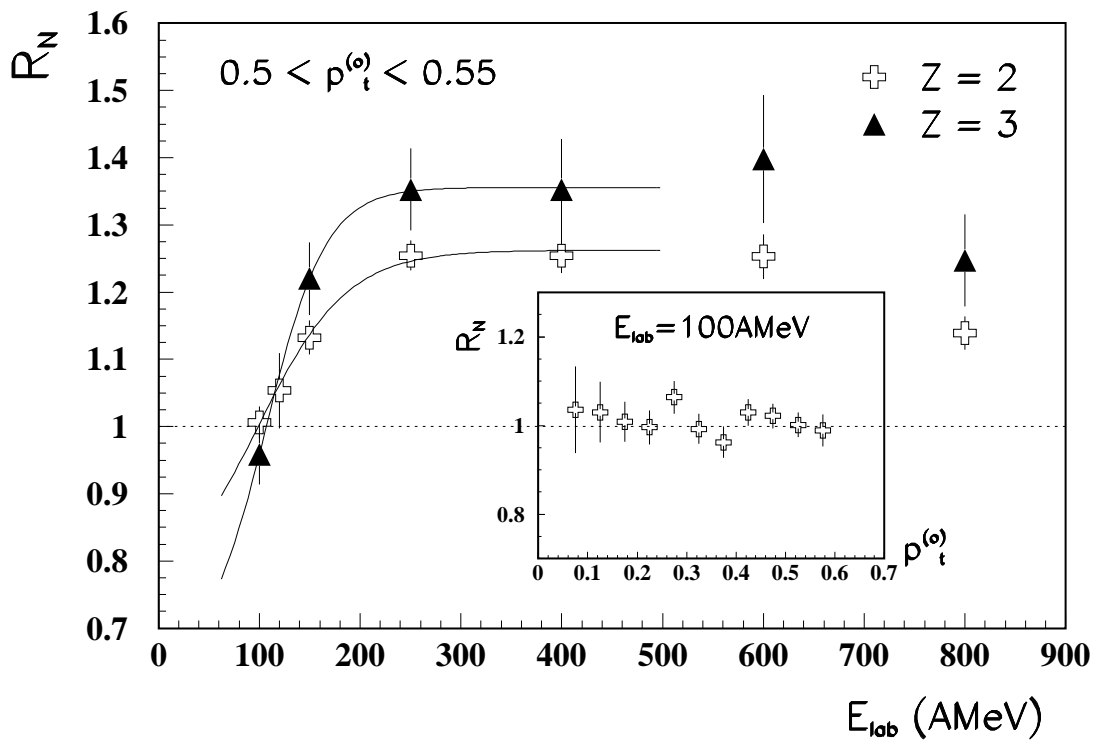


Figure 6

